

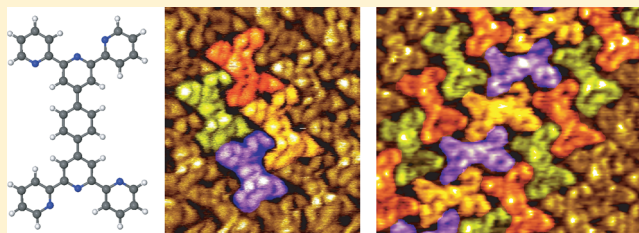
# Experimental and Theoretical Analysis of Hydrogen Bonding in Two-Dimensional Chiral 4',4'''-(1,4-Phenylene)bis(2,2':6',2''-terpyridine) Self-Assembled Nanoarchitecture

Manuela Mura\*<sup>†</sup> and Fabien Silly\*<sup>‡</sup>

<sup>†</sup>Computational Physics Group, School of Mathematics and Physics, University of Lincoln, Brayford Pool, Lincoln LN6 7TS, U.K.

<sup>‡</sup>CEA, IRAMIS, SPEC, TITANS, CNRS, Université Paris-Saclay, F-91191 Gif sur Yvette, France

**ABSTRACT:** The two-dimensional self-assembly of 4',4'''-(1,4-phenylene)bis(2,2':6',2''-terpyridine) molecules is experimentally and theoretically investigated. Scanning tunneling microscopy (STM) shows that this molecular building block forms a compact chiral supramolecular network on graphite at the 1-octanol/graphite interface. The molecules adopt a side-by-side arrangement inside the organic domains. In contrast, the molecules are arranged perpendicularly at the domain boundary. Detailed theoretical analysis based on the density functional theory (DFT) shows that these arrangements are stabilized by double and single hydrogen bonds between pyridine groups. Only the molecular peripheral pyridine groups are involved in the hydrogen bonds stabilizing the long-range ordered molecular nanoarchitectures.



## INTRODUCTION

Engineering novel organic nanoarchitectures through bottom-up strategy and molecular self-assembly<sup>1–16</sup> is attracting increasing interest over the past decade. Predicting and controlling self-assembly is a prerequisite to fabricate well-defined nanoarchitectures with specific local electronic properties.<sup>17–19</sup> Hydrogen bonding is an appealing intermolecular interaction to govern molecular self-assembly due to the high selectivity and high directionality of this bond.<sup>20–27</sup> Imide and carboxylic groups are functional units that can drive molecular self-assembly through the formation of double (N–H···O) or (O–H···O) hydrogen bonds, respectively.<sup>28–30</sup> The pyridine group is an interesting alternative to these substituents because of its flexibility. This group is not only expected to drive molecular self-assembly through the formation of double hydrogen bonds (C–H···N) between neighboring molecules, but the N atom can be located in different position of the benzene ring. The flexibility of this group opens new opportunities to engineer new architectures. Specific pyridine-based molecular building blocks have been recently synthesized<sup>31,32</sup> for application in the fields of supramolecular chemistry and materials science.<sup>31</sup> Hydrogen-bonded two-dimensional nanoarchitectures have been engineered using pyridine-based molecular building blocks.<sup>33,34</sup> The conformation of terpyridine compounds can change in organic nanoarchitectures according to Wang et al.<sup>35</sup> Perypheral pyridine groups can adopt a *trans* or *cis* conformation to confer stability to the molecular self-assembly. However, the strength of molecular bonds has not yet been assessed in terpyridine-compound self-assembly.

In this paper, we investigate the self-assembly of 4',4'''-(1,4-phenylene)bis(2,2':6',2''-terpyridine) molecules at the 1-

octanol/graphite interface. Scanning tunneling microscopy (STM) reveals that the molecules self-assembled into a two-dimensional close-packed chiral nanoarchitecture. Molecules are arranged side-by-side inside the molecular domain whereas molecular are arranged perpendicularly at the domain boundary. Density functional theory (DFT) modeling reveals that this structures is stabilized by double and single hydrogen bonds between pyridine groups.

## EXPERIMENTAL AND THEORETICAL METHODS

Solutions of 4',4'''-(1,4-phenylene)bis(2,2':6',2''-terpyridine) in 1-octanol (99%, Acros) were prepared. A droplet of this solution was then deposited on a graphite substrate. STM imaging of the samples was performed at the liquid/solid interface<sup>36</sup> using a Pico-SPM (Molecular Imaging, Agilent Technology) scanning tunneling microscope. Cut Pt/Ir tips were used to obtain constant current images at room temperature with a bias voltage applied to the sample. STM images were processed and analyzed using the application FabViewer.<sup>37</sup>

To model the molecular arrangement of the calculations 4',4'''-(1,4-phenylene)bis(2,2':6',2''-terpyridine) molecules simulations were performed using the *ab initio* SIESTA package.<sup>38</sup> SIESTA is based on the localized numerical orbital basis set, periodic boundary conditions, and the first-principles scalar-relativistic norm-conserving Troullier–Martins<sup>39</sup> pseudo-potential factorized in the Kleinman–Bylander<sup>40</sup> form. We

Received: July 26, 2015

Revised: September 25, 2015

77 used Perdew, Becke, and Ernzerhof (PBE)<sup>41</sup> generalized  
 78 gradient approximation for the exchange and correlation,  
 79 which was found previously to be adequate in representing  
 80 hydrogen bonding between DNA base molecules.<sup>42</sup> In each  
 81 calculation, atomic relaxation was performed until forces on  
 82 atoms were less than 0.01 eV/Å in the cases of dimers and 0.03  
 83 eV/Å in the cases of monolayers. The effect of the vdW forces  
 84 in the assembly of molecules on the surface has been  
 85 considered thanks to the vdW-DF *ab initio* method.<sup>43–45</sup> The  
 86 energetics of each gas-phase monolayer, calculated using  
 87 SIESTA, is characterized by its stabilization energy, which is  
 88 composed of two components: the interaction and deformation  
 89 energies. If the former characterizes the strength of  
 90 intermolecular interaction (it is negative), the latter shows  
 91 the energy penalty due to inevitable deformation of molecules  
 92 in the final structure (and is positive). The calculated energies  
 93 include the basis set superposition error (BSSE) correction<sup>46</sup>  
 94 due to the localized basis set used. To analyze bonding in the  
 95 relaxed structures, the electron density difference (between the  
 96 total density and that of all individual molecules in the  
 97 geometry of the combined system) was found to be especially  
 98 useful because the hydrogen bonding is known to be well  
 99 characterized by the “kebab” structure associated with  
 100 alternating regions of excess and depletion of the electron  
 101 density along the donor–hydrogen–acceptor line of atoms.<sup>42</sup>

## 102 ■ RESULTS AND DISCUSSION

103 The chemical structure of the 4',4'''-(1,4-phenylene)bis-  
 104 (2,2':6',2''-terpyridine) molecule is presented in Figure 1.  
 105 This 2-fold symmetry molecule is a H-shaped molecule. Its  
 106 skeleton consists of a central benzene ring connected to two  
 107 peripheral terpyridine groups.

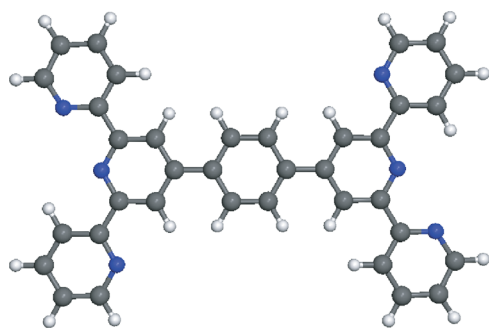


Figure 1. 4',4'''-(1,4-Phenylene)bis(2,2':6',2''-terpyridine) molecule (C<sub>36</sub>H<sub>24</sub>N<sub>6</sub>). Carbon atoms are gray, hydrogen atoms are white, and nitrogen atoms are blue, respectively.

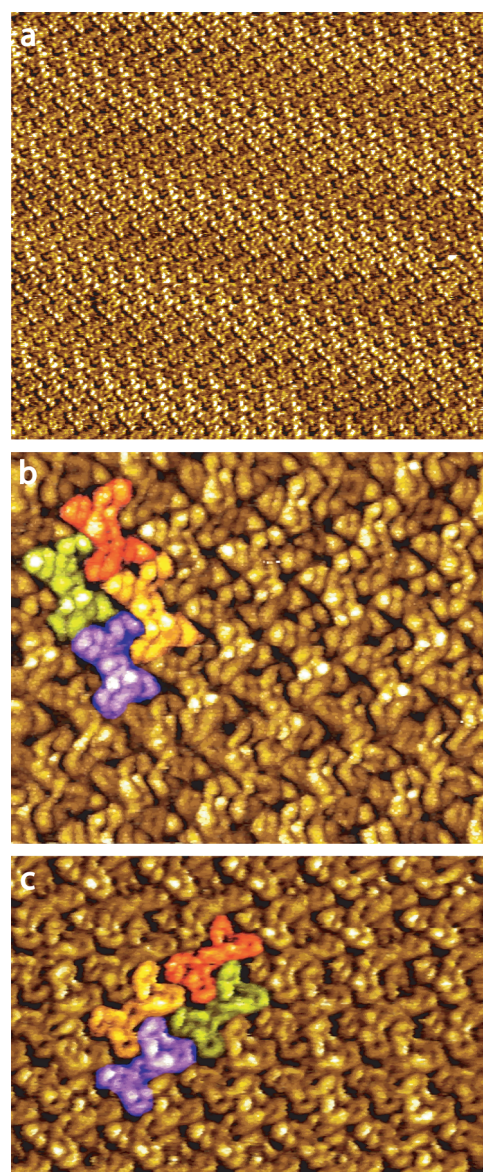


Figure 2. (a) Large scale STM image of 4',4'''-(1,4-phenylene)bis-(2,2':6',2''-terpyridine) chiral nanoarchitecture on graphite, 30 × 26 nm<sup>2</sup>; V<sub>s</sub> = 0.5 V, I<sub>t</sub> = 180 pA. The two enantiomeric domains are presented in the high-resolution STM images: (b) 9 × 8 nm<sup>2</sup>, V<sub>s</sub> = 0.5 V, I<sub>t</sub> = 180 pA; (c) 9 × 7 nm<sup>2</sup>, V<sub>s</sub> = 0.5 V, I<sub>t</sub> = 180 pA. Molecules comprising the unit cell are in red, green, blue, and yellow in (b) and (c).

108 Figure 2a, the large scale STM image, reveals that 4',4'''-(1,4-  
 109 phenylene)bis(2,2':6',2''-terpyridine) molecules self-assemble  
 110 into large close-packed nanoarchitectures at the 1-octanol/  
 111 graphite interface. The molecules are entirely covering the  
 112 graphite surface. This molecular arrangement is chiral and is  
 113 stable during STM imaging. The two enantiomeric structures  
 114 are visible in the high resolution STM images presented in  
 115 Figure 2b,c. Intramolecular features corresponding to the  
 116 integrated density of states of the molecule appear distinctly in  
 117 the high resolution STM images, Figure 2b,c. The molecules  
 118 forming the chiral network unit cells have been colored in  
 119 yellow, red, blue, and green as a guide for the eyes. Neighboring  
 120 molecules are arranged parallel to each other. The model of this  
 121 self-assembled nanoarchitecture is presented in Figure 4a. The

network unit cell of this close-packed structure is a parallelo- 122  
 gram with  $2.0 \pm 0.2$  and  $1.4 \pm 0.2$  nm unit cell constants ( $A_1$ , 123  
 $A_2$ ) and an angle  $\theta$  of  $67 \pm 3^\circ$  between the axes, Table 1. 124 11  
 The lattice vectors ( $A_1$ ,  $A_2$ ) are represented by purple arrows in 125  
 Figure 4a. 126

An STM image of the domain boundary is presented in 127  
 Figure 3. The molecules at the edge of the domains have been 128 13  
 colored in red and green, as a guide for the eyes. The molecules 129  
 of neighboring domains are aligned (red, green molecules). The 130  
 two domains are separated by a molecular row (molecules 131  
 colored in yellow and blue). The molecules of this row are 132  
 parallel to each other, but they are rotated by  $80^\circ$  with respect 133  
 to the molecules of the domains. The molecules of the side-by- 134  
 side arrangement are epitaxially oriented on the graphite 135  
 surface. The perpendicular molecules are in contrast aligned in 136

**Table 1. Unit Cell Parameters: Lengths of the Two Lattice Vectors ( $A_1$ ,  $A_2$ ) and the Angle  $\theta$  between Them for the  $4',4''''$ -(1,4-Phenylene)bis(2,2':6',2''-terpyridine) Nanoarchitecture<sup>a</sup>**

phase technique:	parallel		perpendicular	
	STM	DFT	STM	DFT
$A_1$ (Å)	20	18.8	34	31.5
$A_2$ (Å)	14	13.4	14	12.9
$\theta$ (deg)	67	65	85	89
$\tau$ (deg)	0	0	77	77

<sup>a</sup>The difference in the orientations of the two molecules within the cell is shown by the angle  $\tau$ .

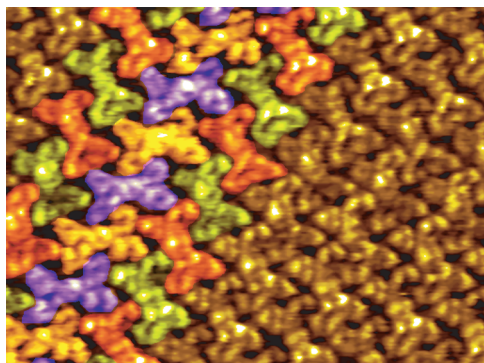


**Figure 3.** STM image of the  $4',4''''$ -(1,4-phenylene)bis(2,2':6',2''-terpyridine) nanoarchitecture domain boundary,  $10 \times 8 \text{ nm}^2$ ;  $V_s = 0.5 \text{ V}$ ,  $I_t = 180 \text{ pA}$ . Molecules of the domain edge are in red and green. Molecules separating the neighboring domains are in yellow and blue.

another crystalline direction of the graphite surface. The network unit cell at the domain boundary is represented by a purple dashed line in the model shown in Figure 5a. The boundary unit cell is a parallelogram with  $3.4 \pm 0.3$  and  $1.4 \pm 0.3 \text{ nm}$  unit cell constants and an angle  $\theta$  of  $85 \pm 4^\circ$  between the axes, Table 1. The lattice vectors ( $A_1$ ,  $A_2$ ) are represented by purple arrows in Figure 5a.

Hoster et al. previously investigated the hydrogen-bonding in bis(terpyridine) derivative arrangements.<sup>47</sup> They theoretically estimated intermolecular interaction by modeling the interaction of free benzene and pyridine rings. Their calculations show that  $\text{N}\cdots\text{H}$  interaction energy is drastically stronger than  $\text{H}\cdots\text{H}$  interaction. Their model, however, does not take into account the whole molecular structure. It was also assumed that

the molecules were adopting a planar configuration in these calculations.

In our calculations, the whole molecular structure is modeled and the possibility that molecular structure can adopt different configurations is also taken into account. For the parallel and perpendicular networks, two unit cells were considered. The unit cells are composed of two and four molecules, respectively. The two geometries reveal a similar stabilization energy and energy per molecule for the two nanoarchitectures (Table 2). The perpendicular arrangement of molecular dimers is slightly more stable than the parallel configuration when two molecules are considered. In contrast, the perpendicular arrangement appears to be less stable when four molecules in the unit cell are considered (Table 2). The density of the perpendicular arrangement ( $0.47 \text{ mol/nm}^2$ ) is slightly larger than the one of the parallel arrangement ( $0.44 \text{ mol/nm}^2$ ). In fact, the perpendicular configuration of tetramers becomes less stable because it induces a distortion of molecular conformation in the unit cell. The molecular peripheral pyridine groups are rotating with respect to the molecular plane; i.e., the terpyridine groups are then not flat. This rotation weakens the hydrogen bond between neighboring molecules and increases the energy of the molecular arrangement.

The calculations reveal that the unit cell (containing one molecule) of the parallel arrangement is stabilized by two double H-bonds highlighted by dark blue circles in Figure 4c. In comparison, the monolayer based on the perpendicular tetramers (Figure 5c) contains two molecules per unit cell, which is stabilized by two double H-bond (dark blue circles) and two single H-bonds (light blue circles), Figure 5c. The gray circle highlights a charge rearrangement, which does not correspond to a H-bond. The unit cell of the parallel arrangement is therefore stabilized by a higher number of H-bonds per molecules than the unit cell of the perpendicular arrangement. However, calculations only reveal a small difference in energy between the two assemblies (Table 3), which indicates that the hydrogen bonds between neighboring molecules are stronger in the perpendicular tetramer than in the aligned tetramers when the monolayer is formed. The difference in strength between the two assemblies can be observed in the “kebab” plot in Figures 4 and 5. In these plots, the alternating regions of depletion and excess of the density along the H-bonds characterize the strength of the bonding. The molecules are bonded to each other through two  $\text{N}\cdots\text{H}-\text{C}$  bonds between their peripheral terpyridine groups in the parallel arrangement, Figure 4b. In contrast, the N atom of the molecular central terpyridine group is not involved in any H-

**Table 2. Calculated Energies: Building Blocks and Calculated Energies of the  $4',4''''$ -(1,4-Phenylene)bis(2,2':6',2''-terpyridine) Networks (PBE, BSSE, and Cohesion Energies,  $E_{\text{coh}}$ )**

Structure	Parallel		Perpendicular	
	Dimer	Tetramer	Dimer	Tetramer
Molecular block				
Energy (eV)				
(PBE)	-0.35	-0.87	-0.41	-0.63
BSSE Energy (eV)	0.04	0.2	0.04	0.2
$E_{\text{coh}}$ (eV)				
per molecule	0.18	0.22	0.21	0.16

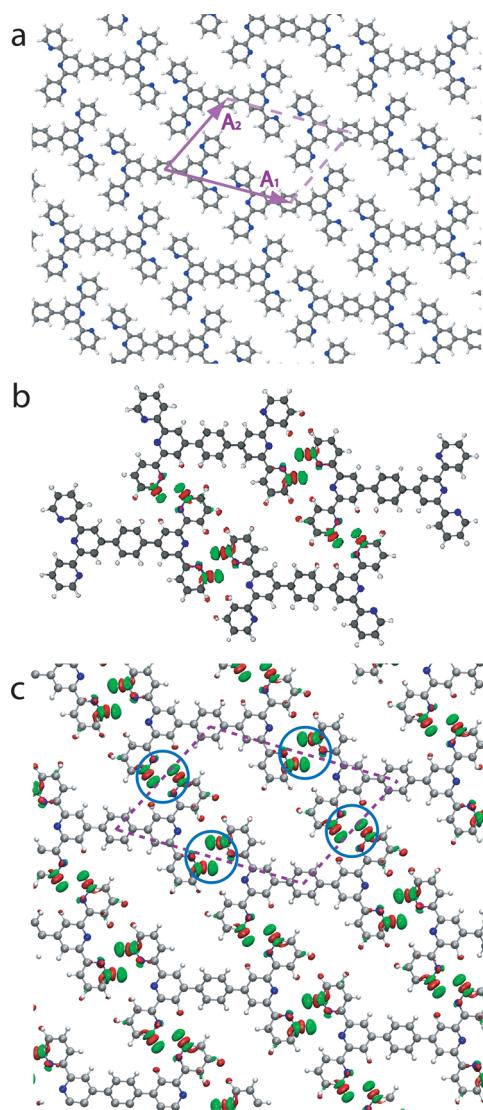


**Figure 4.** (a) Model of the 4',4'''-(1,4-phenylene)bis(2,2':6',2''-terpyridine) nanoarchitecture. The lattice vectors  $A_1$  and  $A_2$  are indicated by arrows, and the unit cell is indicated by a dashed box for convenience. (b) Geometries of the 4',4'''-(1,4-phenylene)bis(2,2':6',2''-terpyridine) tetramer shown together with the electron density difference plots corresponding to  $\pm 0.005 \text{ \AA}^{-3}$ . The green surfaces correspond to the regions of positive electron density difference (excess) and the red areas correspond to the regions of negative electron density difference (depletion). (c) Electron density difference plot of the molecular network.

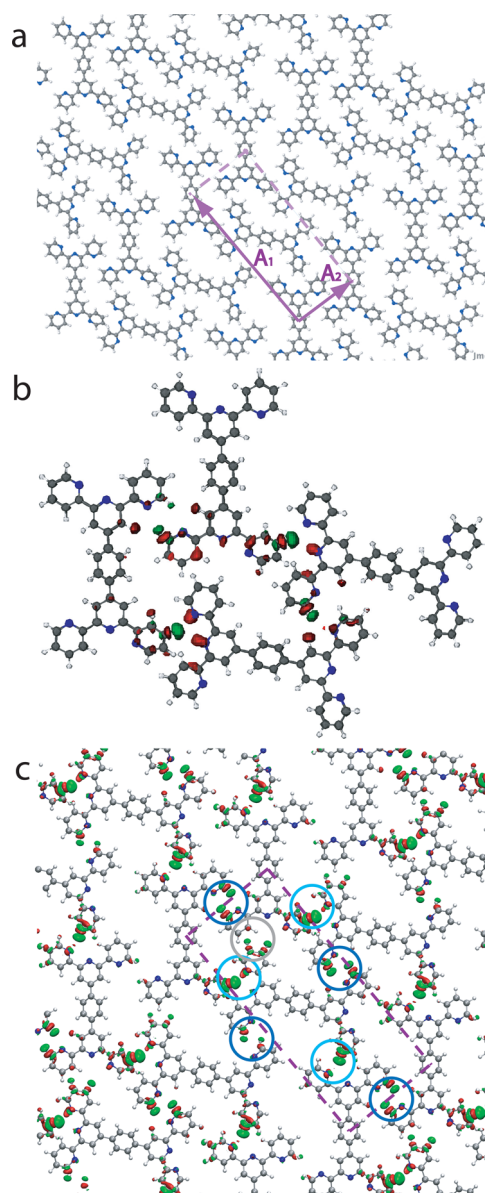


**Figure 5.** Geometries of the 4',4'''-(1,4-phenylene)bis(2,2':6',2''-terpyridine) tetramer shown together with the electron density difference plots corresponding to  $\pm 0.005 \text{ \AA}^{-3}$ . The green surfaces correspond to the regions of positive electron density difference (excess), and the red areas correspond to the regions of negative electron density difference (depletion). (c) Electron density difference plot of the molecular perpendicular arrangement.

**Table 3. Cohesion Energies: Number of Molecules per Unit Cell and Calculated Cohesion Energies  $E_{\text{coh}}$  per Molecule of the 4',4'''-(1,4-Phenylene)bis(2,2':6',2''-terpyridine) Network**

structure	parallel	perpendicular
energy (eV) (PBE)	-1.16	-1.06
B SSE energy (eV)	0.28	0.30
$E_{\text{coh}}$ (eV)	-0.29	-0.27

observations, Table 1. The perpendicular configuration does, 212 however, present some slight differences. These are probably 213 induced by the molecular distortion, which leads to a noticeable 214 nonplanar configuration. The presence of a surface is expected 215 to reduce this effect and limit the variation of molecular 216

198 bond. In comparison, the central pyridine group is forming a H-  
199 bond with the peripherical pyridine group of a neighboring  
200 molecule in the perpendicular arrangement, when only four  
201 molecules are considered, Figure 5b. It should be noticed that  
202 the electrostatic plot shows an incomplete “kebab” in the  
203 proximity of the nitrogen atom of each terpyridine groups,  
204 which underlines the weakness of this bond. The calculations  
205 presented in Figure 5c reveal that the central pyridine group is  
206 not involved in H-bonding when the tetramer periodic images  
207 are chosen to interact between each other to mimic the  
208 monomer periodic structure experimentally observed in Figure  
209 3.

210 The calculated gas-phase close-packed and perpendicular  
211 configurations are in good agreement with experimental

217 conformation in comparison with the gas-phase configuration.  
218 In contrast, the parallel arrangement is expected to be less  
219 influenced by the presence of the surface as the molecular  
220 distortion is smaller in this structure. In addition, these  
221 molecules appear to be aligned in a preferential direction of  
222 the graphite surface (epitaxial domains). This is not the case for  
223 the perpendicular molecules. The experimental stabilization  
224 energy of this perpendicular arrangement will therefore  
225 decrease and so be less favorable when compared with that  
226 of the parallel arrangement. This explains, therefore, why the  
227 perpendicular arrangement is only locally observed at the  
228 domain boundary in the STM images. It should be noticed that  
229 a Moiré pattern can be observed in the STM images for the  
230 parallel arrangement. This suggests some electronic coupling  
231 between the molecules and the substrate,<sup>48</sup> but this also reveals  
232 that there is no preferential adsorption site for the molecules  
233 along the graphite direction.

## 234 ■ CONCLUSION

235 In this paper we investigated the two-dimensional self-assembly  
236 of 4',4'''-(1,4-phenylene)bis(2,2':6',2''-terpyridine) on a graph-  
237 ite surface. Molecules adopt a side-by-side arrangement inside  
238 the monolayer but are arranged perpendicularly at the domain  
239 boundary. Experimental observations and calculations reveal  
240 that the molecule forms a close-packed structure stabilized by  
241 double and single hydrogen-bonds. Calculations show that the  
242 molecular conformation is less planar in the perpendicular  
243 molecular packing than in the molecular parallel packing. The  
244 flexibility of terpyridine groups open new opportunities to  
245 engineer new organic nanoarchitectures on surfaces.

## 246 ■ AUTHOR INFORMATION

### 247 Corresponding Authors

248 \*E-mail: mmura@lincoln.ac.uk. Phone: +44 (0)1522835866.

249 \*E-mail: fabien.silly@cea.fr. Phone: +33(0)169088019. Fax:  
250 +33(0)169088446.

### 251 Notes

252 The authors declare no competing financial interest.

## 253 ■ ACKNOWLEDGMENTS

254 The research leading to these results has received funding from  
255 the European Research Council under the European Union's  
256 Seventh Framework Programme (FP7/2007-2013)/ERC grant  
257 agreement no. 259297.

## 258 ■ REFERENCES

- 259 (1) Shang, J.; Wang, Y.; Chen, M.; Dai, J.; Zhou, X.; Kuttner, J.; Hilt,  
260 G.; Shao, X.; Gottfried, J. M.; Wu, K. Assembling Molecular Sierpiński  
261 Triangle Fractals. *Nat. Chem.* **2015**, *7*, 389–393.  
262 (2) Pawin, G.; Wong, K. L.; Kwon, K.-Y.; Bartels, L. A  
263 Homomolecular Porous Network at a Cu(111) Surface. *Science* **2006**,  
264 *313*, 961–962.  
265 (3) Wu, R.; Yan, L.; Zhang, Y.; Ren, J.; Bao, D.; Zhang, H.; Wang, Y.;  
266 Du, S.; Huan, Q.; Gao, H.-J. Self-Assembled Patterns and Young's  
267 Modulus of Single-Layer Naphthalocyanine Molecules on Ag(111). *J.*  
268 *Phys. Chem. C* **2015**, *119*, 8208–8212.  
269 (4) Wang, Q. H.; Hersam, M. C. Room-Temperature Molecular-  
270 Resolution Characterization of Self-Assembled Organic Monolayers on  
271 Epitaxial Graphene. *Nat. Chem.* **2009**, *1*, 206–211.  
272 (5) Lu, J.; Yeo, P. S. E.; Zheng, Y.; Yang, Z.; Bao, Q.; Gan, C. K.; Loh,  
273 K. P. Using the Graphene Moiré Pattern for the Trapping of C<sub>60</sub> and  
274 Homoepitaxy of Graphene. *ACS Nano* **2012**, *6*, 944–950.  
275 (6) Maeda, H. Supramolecular Chemistry of Pyrrole-Based  $\pi$ -  
276 Conjugated Molecules. *Bull. Chem. Soc. Jpn.* **2013**, *86*, 1359–1399.

- (7) Amrous, A.; Bocquet, F.; Nony, L.; Para, F.; Loppacher, C.; 277  
Lamare, S.; Palmino, F.; Cherioux, F.; Gao, D. Z.; Canova, F. F.; et al. 278  
Molecular Design and Control Over the Morphology of Self- 279  
Assembled Films on Ionic Substrates. *Adv. Mater. Interfaces* **2014**, *1*, 280  
1400414. 281  
(8) Uemura, S.; Aono, M.; Sakata, K.; Komatsu, T.; Kunitake, M. 282  
Thermodynamic Control of 2D Bicomponent Porous Networks of 283  
Melamine and Melem: Diverse Hydrogen-Bonded Networks. *J. Phys.* 284  
*Chem. C* **2013**, *117*, 24815–24821. 285  
(9) Kikkawa, Y.; Ishitsuka, M.; Kashiwada, A.; Tsuzuki, S.; Hiratani, 286  
K. Bicomponent Blend-Directed Amplification of the Alkyl Chain 287  
Effect on the 2D Structures. *Chem. Commun.* **2014**, *50*, 13146–13149. 288  
(10) Li, M.; Zeng, Q.; Wang, C. Self-Assembled Supramolecular 289  
Networks at Interfaces: Molecular Immobilization and Recognition 290  
Using Nanoporous Templates. *Sci. China: Phys., Mech. Astron.* **2011**, 291  
*54*, 1739–1748. 292  
(11) Liang, H.; He, Y.; Ye, Y.; Xu, X.; Cheng, F.; Sun, W.; Shao, X.; 293  
Wang, Y.; Li, J.; Wu, K. Two-Dimensional Molecular Porous Networks 294  
Constructed by Surface Assembling. *Coord. Chem. Rev.* **2009**, *253*, 295  
2959–2979. 296  
(12) Otsuki, J. STM Studies on Porphyrins. *Coord. Chem. Rev.* **2010**, 297  
*254*, 2311–2341. 298  
(13) Rosei, F.; Schunack, M.; Naitoh, Y.; Jiang, P.; Gourdon, A.; 299  
Laegsgaard, E.; Stensgaard, I.; Joachim, C.; Besenbacher, F. Properties 300  
of Large Organic Molecules on Metal Surfaces. *Prog. Surf. Sci.* **2003**, 301  
*71*, 95–146. 302  
(14) Roy, B.; Bairi, P.; Nandi, A. K. Supramolecular Assembly of 303  
Melamine and its Derivatives: Nanostructures to Functional Materials. 304  
*RSC Adv.* **2014**, *4*, 1708–1734. 305  
(15) Yagai, S. Supramolecularly Engineered Functional  $\pi$ -Assemblies 306  
Based on Complementary Hydrogen-Bonding Interactions. *Bull.* 307  
*Chem. Soc. Jpn.* **2015**, *88*, 28–58. 308  
(16) Yang, Y.; Wang, C. Hierarchical Construction of Self-Assembled 309  
Low-Dimensional Molecular Architectures Observed by Using 310  
Scanning Tunneling Microscopy. *Chem. Soc. Rev.* **2009**, *38*, 2576. 311  
(17) Hieulle, J.; Silly, F. Localized Intermolecular Electronic 312  
Coupling in Two-Dimensional Self-Assembled 3,4,9,10-perylene-tetra- 313  
carboxylic Diimide Nanoarchitectures. *J. Mater. Chem. C* **2013**, *1*, 314  
4536–4539. 315  
(18) Sedona, F.; Marino, M. D.; Forrer, D.; Vittadini, A.; Casarin, M.; 316  
Cossaro, A.; Floreano, L.; Verdini, A.; Sami, M. Tuning the catalytic 317  
activity of Ag(110)-supported Fe phthalocyanine in the oxygen 318  
reduction reaction. *Nat. Mater.* **2012**, *11*, 970–977. 319  
(19) Gusev, A. O.; Taleb, A.; Silly, F.; Charra, F.; Pileni, M.-P. 320  
Inhomogeneous Photon Emission Properties of Self-Assembled 321  
Metallic Nanocrystals. *Adv. Mater.* **2000**, *12*, 1583–1587. 322  
(20) Yagai, S.; Goto, Y.; Lin, X.; Karatsu, T.; Kitamura, A.; Kuzuhara, 323  
D.; Yamada, H.; Kikkawa, Y.; Saeki, A.; Seki, S. Self-Organization of 324  
Hydrogen-Bonding Naphthalene Chromophores into J-type Nanorings 325  
and H-type Nanorods: Impact of Regioisomerism. *Angew. Chem.,* 326  
*Int. Ed.* **2012**, *51*, 6643–6647. 327  
(21) Barth, J. V. Molecular Architectonics on Metal Surfaces. *Annu.* 328  
*Rev. Phys. Chem.* **2007**, *58*, 375–407. 329  
(22) Mura, M.; Sun, X.; Silly, F.; Jonkman, H. T.; Briggs, G. A. D.; 330  
Castell, M. R.; Kantorovich, L. N. Experimental and Theoretical 331  
Analysis of H-Bonded Supramolecular Assemblies of PTCDA 332  
Molecules. *Phys. Rev. B: Condens. Matter Mater. Phys.* **2010**, *81*, 333  
195412. 334  
(23) Yagai, S.; Iwai, K.; Yamauchi, M.; Karatsu, T.; Kitamura, A.; 335  
Uemura, S.; Morimoto, M.; Wang, H.; Würthner, F. Photocontrol 336  
Over Self-Assembled Nanostructures of  $\pi$ - $\pi$  Stacked Dyes Supported 337  
by the Parallel Conformer of Diarylethene. *Angew. Chem., Int. Ed.* 338  
**2014**, *53*, 2602–2606. 339  
(24) De Feyter, S.; De Schryver, F. C. Two-Dimensional Supra- 340  
molecular Self-Assembly Probed by Scanning Tunneling Microscopy. 341  
*Chem. Soc. Rev.* **2003**, *32*, 139–150. 342  
(25) Sun, X.; Jonkman, H. T.; Silly, F. Tailoring Two-Dimensional 343  
PTCDA-melamine Self-Assembled Architectures at Room Temper- 344  
ature by Tuning Molecular Ratio. *Nanotechnology* **2010**, *21*, 165602. 345

- 346 (26) Bonifazi, D.; Mohnani, S.; Llanes-Pallas, A. Supramolecular  
347 Chemistry at Interfaces: Molecular Recognition on Nanopatterned  
348 Porous Surfaces. *Chem. - Eur. J.* **2009**, *15*, 7004–7025.
- 349 (27) Mura, M.; Silly, F.; Burlakov, V.; Castell, M. R.; Briggs, G. A. D.;  
350 Kantorovich, L. N. Formation Mechanism for a Hybrid Supra-  
351 molecular Network Involving Cooperative Interactions. *Phys. Rev. Lett.*  
352 **2012**, *108*, 176103.
- 353 (28) Hu, F.-Y.; Zhang, X.-M.; Wang, X.-C.; Wang, S.; Wang, H.-Q.;  
354 Duan, W.-B.; Zeng, Q.-D.; Wang, C. In Situ STM Investigation of  
355 Two-Dimensional Chiral Assemblies through Schiff-Base Condensa-  
356 tion at a Liquid/Solid Interface. *ACS Appl. Mater. Interfaces* **2013**, *5*,  
357 1583–1587.
- 358 (29) Suh, M. P.; Cheon, Y. E.; Lee, E. Y. Syntheses and Functions of  
359 Porous Metallosupramolecular Networks. *Coord. Chem. Rev.* **2008**,  
360 *252*, 1007–1026.
- 361 (30) Zhang, X.; Zeng, Q.; Wang, C. Molecular Templates and Nano-  
362 Reactors: Two-Dimensional Hydrogen Bonded Supramolecular Net-  
363 works on Solid/Liquid Interfaces. *RSC Adv.* **2013**, *3*, 11351–11366.
- 364 (31) Wild, A.; Winter, A.; Schlütter, F.; Schubert, U. S. Advances in  
365 the Field of  $\pi$ -Conjugated 2,2':6',2''-terpyridines. *Chem. Soc. Rev.*  
366 **2011**, *40*, 1459–1511.
- 367 (32) Earmme, T.; Jenekhe, S. A. Solution-Processed, Alkali Metal-  
368 Salt-Doped, Electron-Transport Layers for High-Performance Phos-  
369 phorescent Organic Light-Emitting Diodes. *Adv. Funct. Mater.* **2012**,  
370 *22*, 5126–5136.
- 371 (33) Roos, M.; Künzel, D.; Uhl, B.; Huang, H.-H.; Brandao Alves, O.;  
372 Hoster, H. E.; Gross, A.; Behm, R. J. Hierarchical Interactions and  
373 Their Influence upon the Adsorption of Organic Molecules on a  
374 Graphene Film. *J. Am. Chem. Soc.* **2011**, *133*, 9208–9211.
- 375 (34) Meier, C.; Landfester, K.; Ziener, U. Adsorbate-Substrate-  
376 Mediated Growth of Oligopyridine Monolayers at the Solid/Liquid  
377 Interface. *J. Phys. Chem. C* **2009**, *113*, 1507–1514.
- 378 (35) Wang, S.; Zhao, F.; Luo, S.; Geng, Y.; Zeng, Q.; Wang, C.  
379 Solvent-Induced Variable Conformation of Bis(terpyridine) Deriva-  
380 tives During Supramolecular Self-Assembly at Liquid/HOPG Inter-  
381 faces. *Phys. Chem. Chem. Phys.* **2015**, *17*, 12350–12355.
- 382 (36) Silly, F. Selecting Two-Dimensional Halogen-Halogen Bonded  
383 Self-Assembled 1,3,5-Tris(4-iodophenyl)benzene Porous Nanoarchi-  
384 tectures at the Solid-Liquid Interface. *J. Phys. Chem. C* **2013**, *117*,  
385 20244–20249.
- 386 (37) Silly, F. A Robust Method For Processing Scanning Probe  
387 Microscopy Images and Determining Nanoobject Position and  
388 Dimensions. *J. Microsc.* **2009**, *236*, 211–218.
- 389 (38) Sánchez-Portal, D.; Ordejón, P.; Artacho, E.; Soler, J. M.  
390 Density-Functional Method for Very Large Systems with LCAO Basis  
391 Sets. *Int. J. Quantum Chem.* **1997**, *65*, 453–461.
- 392 (39) Troullier, N.; Martins, J. L. Efficient Pseudopotentials for Plane-  
393 Wave Calculations. *Phys. Rev. B: Condens. Matter Mater. Phys.* **1991**, *43*,  
394 1993.
- 395 (40) Kleinman, L. Relativistic Norm-Conserving Pseudopotential.  
396 *Phys. Rev. B: Condens. Matter Mater. Phys.* **1980**, *21*, 2630.
- 397 (41) Perdew, J. P.; Burke, K.; Ernzerhof, M. Generalized Gradient  
398 Approximation Made Simple. *Phys. Rev. Lett.* **1996**, *77*, 3865–3868.
- 399 (42) Kelly, R. E. A.; Lee, Y. J.; Kantorovich, L. N. Homopairing  
400 Possibilities of the DNA Bases Cytosine and Guanine: An ab Initio  
401 DFT Study. *J. Phys. Chem. B* **2005**, *109*, 22045–22052.
- 402 (43) Dion, M.; Rydberg, H.; Schröder, E.; Langreth, D. C.;  
403 Lundqvist, B. I. Van der Waals Density Functional for General  
404 Geometries. *Phys. Rev. Lett.* **2004**, *92*, 246401.
- 405 (44) Thonhauser, T.; Cooper, V. R.; Li, S.; Puzder, A.; Hyldgaard, P.;  
406 Langreth, D. C. Van der Waals Density Functional: Self-Consistent  
407 Potential and the Nature of the van der Waals Bond. *Phys. Rev. B:*  
408 *Condens. Matter Mater. Phys.* **2007**, *76*, 125112.
- 409 (45) Cooper, V. R.; Thonhauser, T.; Puzder, A.; Schröder, E.;  
410 Lundqvist, B. I.; Langreth, D. C. Stacking Interactions and the Twist of  
411 DNA. *J. Am. Chem. Soc.* **2008**, *130*, 1304–1308.
- 412 (46) Boys, S. F.; Bernardi, F. The Calculation of Small Molecular  
413 Interactions by the Differences of Separate Total Energies. Some  
414 Procedures with Reduced Errors. *Mol. Phys.* **1970**, *19*, 553–566.
- (47) Hoster, H. E.; Roos, M.; Breitruck, A.; Meier, C.; Tonigold, K.;  
415 Waldmann, T.; Ziener, U.; Landfester, K.; Behm, R. J. Structure  
416 Formation in Bis(terpyridine) Derivative Adlayers: Molecule-Substrate  
417 versus Molecule-Molecule Interactions. *Langmuir* **2007**, *23*, 11570–  
418 11579. 419
- (48) Silly, F. Moiré Pattern Induced by the Electronic Coupling  
420 Between 1-Octanol Self-Assembled Monolayers and Graphite Surface.  
421 *Nanotechnology* **2012**, *23*, 225603. 422